

# High-pressure and temperature investigations of energetic materials

**J C Gump**

Naval Surface Warfare Center, Indian Head EOD Technology Division, Indian Head, MD 20640

Email: gumpjc@yahoo.com

**Abstract.** Static high-pressure measurements are extremely useful for obtaining thermodynamic and phase stability information from a wide variety of materials. However, studying energetic materials can be challenging when extracting information from static high-pressure measurements. Energetic materials are traditionally C, H, N, O compounds with low crystalline symmetry, producing weak signal in commonly performed x-ray diffraction measurements. The small sample volume available in a static high-pressure cell exacerbates this issue. Additionally, typical hydrostatic compression media, such as methanol/ethanol, may react with many energetic materials. However, characterization of their thermodynamic parameters and phase stability is critical to understanding explosive performance and sensitivity. Crystalline properties, such as bulk modulus and thermal expansion, are necessary to accurately predict the behaviour of shocked solids using hydrodynamic codes. In order to obtain these values, equations of state of various energetic materials were investigated using synchrotron angle-dispersive x-ray diffraction experiments at static high-pressure and temperature. Intense synchrotron radiation overcomes the weak x-ray scattering of energetic materials in a pressure cell. The samples were hydrostatically compressed using a non-reactive hydrostatic medium and heated using a heated diamond anvil cell. Pressure – volume data for the materials were fit to the Birch-Murnaghan and Vinet formalisms to obtain bulk modulus and its first pressure derivative. Temperature – volume data at ambient pressure were fit to obtain the volume thermal expansion coefficient. Data from several energetic materials will be presented and compared.

## 1. Introduction

Standard explosives typically consist of an energetic ingredient and several non-energetic additives (e.g. plasticisers and binders) that allow for desired processability of the final product (e.g. plasticisers and binders). The energetic ingredient is typically a crystalline, organic (C, H, N, O) material. It is labelled energetic due to its ability to release a large amount of energy over a short time period. Prior to the energy release, most energetics are in a state of high compression or temperature. Thus it is important to investigate the phases of these materials at high pressures or temperatures. To this end heated diamond anvil cells (DACs) offer the ability to investigate these materials.

Standard triggers for energy release from energetic materials are impact, friction, and electrostatic discharge (ESD). The sensitivity threshold for initiation of a given energetic material by one of these sources varies, but working with any energetic material requires safeguards to prevent unintended ignition. This is especially true when applying insults such as high-pressure and temperature to an



energetic sample. An effective way to mitigate the severity of reaction from the energetic material is to work with the smallest quantity necessary. Diamond anvil cells (DACs) provide a means to impart high-pressure and temperature to the samples, but also have an added safety benefit because sample quantities inside a DAC are on the microgram scale.

The objectives of this study were to monitor any phase changes in the crystalline structure of the energetic ingredients studied and to determine certain thermodynamic parameters (bulk modulus, first pressure derivative of the bulk modulus, and volume thermal expansion coefficient). To obtain this information, angle dispersive x-ray diffraction was performed. This report summarizes data collected over approximately ten years, focusing primarily on comparisons between the energetic materials studied and a correlation to shock sensitivity. The energetic materials studied have low crystalline symmetry and poor scattering intensity for x-rays. The small sample size of a DAC reduces signal intensity further. With these limitations, an intense x-ray source is required. Experiments for this study were performed using the Cornell University High Energy Synchrotron Source.

The energetic materials investigated include octahydro-1,3,5,7-tetranitro-1,3,5,7-tetrazocine (HMX)[1], hexanitrohexaazaisowurtzitane (CL-20)[2], 2,6-diamino-3,5-dinitropyrazine-1-oxide (LLM-105)[3], 2,4,6-triamino-1,3,5-trinitrobenzene (TATB)[4], and hexanitrostilbene (HNS)[5]. All of these samples have monoclinic structure, except for TATB, which is triclinic.

## 2. Experimental Procedure

Angle-dispersive x-ray diffraction measurements were performed at the Cornell High Energy Synchrotron Source with a monochromatic ( $\lambda=0.485946$  Å) x-ray beam. DACs were loaded with fine-particle energetic material. A ruby piece ( $\sim 20$   $\mu\text{m}$  in diameter) was added to monitor pressure. The standard methanol/ethanol pressure medium can react with some of the materials studied, so Dow Corning 200 Fluid (5 centistokes), reported to be hydrostatic to 10 GPa [6], was added as a pressure medium for compression experiments in an attempt to create hydrostatic conditions.

High temperatures were achieved by using a hydrothermal diamond anvil cell (HDAC), developed by Bassett et al [7]. In this cell heating coils are in contact with both diamonds. Temperature was monitored by using thermocouples placed near the culet tip of each diamond. Gaskets were made from  $\sim 127$   $\mu\text{m}$  thick Inconel 600 or stainless steel with hole diameters from 150 to 250  $\mu\text{m}$ .

For all experiments an initial diffraction pattern was taken for accurate determination of the sample to detector distance under ambient conditions. For compression measurements, a pressure medium was then added, which typically imposed a slight pressure on the sample. A ruby fluorescence measurement was taken after the addition of fluid to determine sample pressure [8].

At each pressure or temperature, the sample was exposed to incident x-rays for 5-15 minutes and diffracted x-rays were collected by a MAR345 detector. Data were analyzed with SIMPA software [9]. The diffraction peaks were fit to Gaussian waveforms to determine d spacings, and then indexed using the appropriate space group for the energetic material being studied.

## 3. Results and Discussion

### 3.1 Phase Changes

Phase changes in energetic materials are important because of the resulting change in density. Explosive performance metrics (detonation pressure and detonation velocity) are related to the density [10]. Therefore, if a phase change at high pressure results in an increased density then explosive performance could be enhanced if that phase remains stable back to ambient pressure. Of the materials studied in this work, two showed evidence for phase changes within the temperature and pressure ranges explored: HMX and CL-20.

Compression experiments were performed on beta phase HMX at ambient temperature, 100 °C, and 140 °C. Compression up to approximately 6 GPa at ambient temperature and 100 °C, produced no phase change from beta HMX. However, when samples were compressed non-hydrostatically at 140

°C above 4 GPa, decompression resulted in a phase different than the beta phase. Upon comparison with calculated spectra for the known phases of HMX, the decompressed phase matched to that of the delta phase. The diffraction patterns for beta and alpha phases of HMX, typical phases observed in this temperature range, did not match the decompressed pattern. Figure 1 shows the x-ray diffraction patterns upon compression and decompression at 140 °C. A delta phase pattern calculated from single crystal data is included for comparison. The delta phase remained stable to ambient temperature conditions. It is believed that the elevated temperature and non-hydrostatic conditions allowed delta HMX sites to nucleate, which then propagated upon pressure release with the allowed volume expansion.

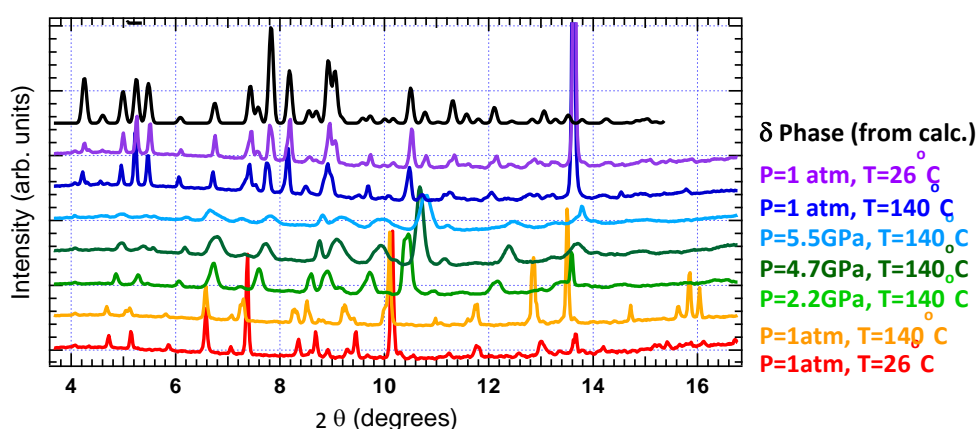


**Figure 1.** X-ray diffraction patterns of HMX at 140 °C compressed to above 5.0 GPa and then decompressed. A calculated delta HMX spectrum is included for comparison.

CL-20 exhibited multiple phase changes in the pressure and temperature regions explored. Results are summarized in figure 2. At ambient temperature, the  $\epsilon$  phase of CL-20 (shown as a solid line) was evident to the highest measure pressure of this study, 5.8 GPa, while the  $\gamma$  phase (shown as a short-dashed line) converts to the  $\zeta$  phase at around 0.9 GPa. The  $\zeta$  phase was previously reported from FTIR measurements at high pressure [11,12], but x-ray confirmation was not obtained. At ambient pressure, the  $\epsilon$  phase is evident to 120 °C, and converts to the  $\gamma$  phase above 125 °C, which when heated above 150 °C resulted in thermal decomposition. The  $\gamma$  phase obtained by 140 °C would convert to the  $\epsilon$  phase upon compression to pressures of merely 0.4 GPa. Upon decompression at 140 °C, the  $\gamma$  phase is recovered, and remains  $\gamma$  after cooling to ambient temperature. The  $\gamma$  phase was compressed at ambient temperature to obtain the  $\zeta$  phase at around 0.9 GPa (shown in figure 2 as a long-dashed line). When heated above 180 °C the  $\zeta$  phase would undergo a phase transformation and decomposition occurred by 240 °C.

### 3.2 Bulk Modulus

Large scale tests on explosive materials pose serious safety concerns due to the violent nature of their reactions. The microsecond reaction time for these materials also makes experimental observation of reaction difficult. Therefore, theoretical models are used to gain insight into explosive reactions. In order for these models to accurately predict explosive performance, thermodynamic parameters for the starting materials should be known. Pressure versus volume data generated from x-ray diffraction data can be used to obtain values for the bulk modulus and its first pressure derivative. This is achieved by fitting the pressure versus volume data to an appropriate equation of state model. Two models have been used to fit the data presented: 3<sup>rd</sup> order Birch-Murnaghan and Vinet. Both models give similar results at ambient temperature and modest pressure [13].

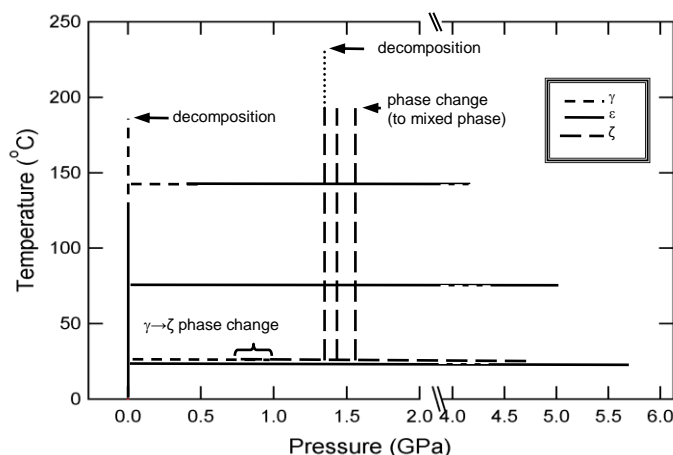


**Figure 2.** Experimental pressure/temperature regions explored for CL-20. Solid lines represent areas where the  $\epsilon$  phase is evident, short-dashed lines represent  $\gamma$  phase regions, and long-dashed lines represent  $\zeta$ . The dashed line at ambient temperature resulted when the starting sample was  $\gamma$ . The dotted line above 200 °C represents a mixed phase resulting from the continued heating of the  $\zeta$  phase.

Figures 3 and 4 provide an illustration of the data and fitting process used to obtain the bulk modulus for the example material of HNS. The unit cell ratios as a function of pressure are shown in figure 3. Compression along the unit cell axes is not uniform in the case of HNS. While the  $a$  and  $b$  axes compress in a similar manner, the  $c$ -axis exhibits no reduction in this range. This asymmetric compression of the unit cell axes occurred for two of the samples investigated: HNS and LLM-105. For LLM-105, the  $b$ -axis shows the least compression. The differences in compression are due to the stacking nature of the lattice planes. This feature and its correlation to explosive sensitivity to impact and friction will be discussed in a later section.

Once the volume is calculated from the unit cell axes at each pressure, the bulk modulus and its first pressure derivative are obtained from fitting the pressure versus volume curve to an equation of state formalism. Figure 4 shows the pressure versus volume data for HNS along with the 3<sup>rd</sup> order Birch-Murnaghan and Vinet equation of state fits. The two fits are so similar at this scale that the lines used to display them are overlapping. It is noted that although the compression of the unit cell axes was very asymmetric, there is no evidence of that appearing in the overall volume compression. The asymmetric nature of the compression is only observed by comparing the compression of the unit cell axes themselves.

Table 1 lists values for the bulk modulus and its first pressure derivative obtained for the materials studied in this work as well as literature values obtained for other materials for comparison [14,15]. Values are listed for gamma CL-20; however, there was limited data available for the fit due to the transition to the zeta phase at such a low pressure. This is reflected in the high percent error in the value obtained for  $K_0'$ . While HMX compression was studied in this work, its ambient temperature values are not listed in the table because the pressure medium used was not Dow Corning 200 fluid and it did not remain hydrostatic throughout the compression experiments. TATB compression values are not listed from this work because there were too few diffraction lines present in the data to get a reasonable fit throughout the compression range. Of the data listed in the table, HNS and LLM-105 exhibit the highest compressibility (lowest bulk modulus). This can probably be correlated to the same lattice plane stacking that is responsible for the asymmetric compression. However, TATB should exhibit a similar trend from its known stacking pattern (discussed later), but its reported bulk modulus is relatively high as compared to the other values in the table.

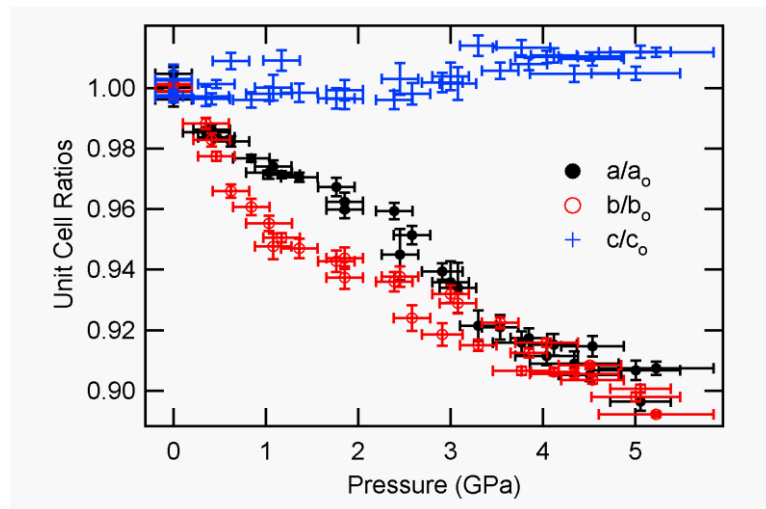


**Figure 3.** Unit cell ratios as a function of pressure for HNS.

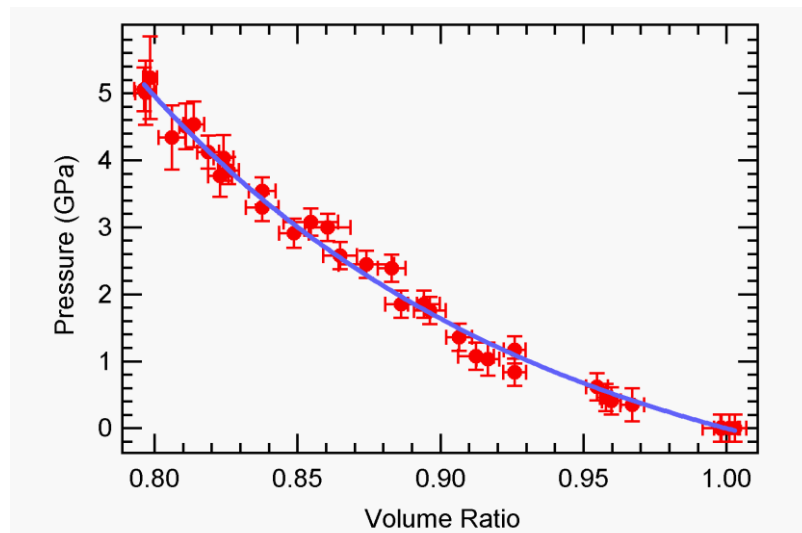


**Figure 4.** Pressure versus volume ratio for HNS. Solid lines represent the 3<sup>rd</sup> order Birch-Murnaghan and Vinet EOS fits to the data (lines are overlapping on this scale).

**Table 1.** Comparison of bulk modulus and its first pressure derivative for samples from this work and from other cited works.

	$K_0$ at amb T (GPa)	$K_0'$ at amb T
$\epsilon$ CL-20	$13.6 \pm 2.0$	$11.7 \pm 3.2$
$\gamma$ CL-20	$18.5 \pm 2.6$	$5.4 \pm 7.9$
LLM-105	$11.19 \pm 0.02$	$18.54 \pm 0.04$
HNS	$11.2 \pm 0.7$	$6.2 \pm 0.7$
HMX (Yoo and Cynn) <sup>14</sup>	12.4	10.4
RDX (Yoo and Cynn) <sup>14</sup>	13.0	6.3
PETN (Yoo and Cynn) <sup>14</sup>	12.3	8.2
TATB (Stevens) <sup>15</sup>	14.7	10.1

### 3.3 Thermal Expansion

The volume thermal expansion coefficient is needed in order to model the response of a material to thermal stimuli, which energetic materials can encounter during ageing and prior to energy release. It can be obtained from a fit to the volume versus temperature data. Figures 5 and 6 illustrate data obtained for HNS from the ambient pressure heating experiments. Asymmetric expansion of the HNS unit cell is evident in figure 5. The a and b axes expand in a similar fashion with temperature, but the c axis shows limited expansion over the temperature range investigated. This correlates with the asymmetric compression data reported in the previous section for HNS. The same lattice plane stacking contributes to both results. This asymmetric expansion of the unit cell axes was also observed for LLM-105 and TATB.

Table 2 lists volume thermal expansion coefficient values obtained from this work and other cited works [16, 17, 18]. There does not appear to be any trend in the thermal expansion coefficient that reflects the asymmetric unit cell expansion. Evidence for asymmetric expansion is only evident from compression curves comparing the individual axes. Comparison of the value obtained in this work for TATB and the reported value from single crystal data from Herman [18] differ by a factor of approximately two. This may reflect the asymmetric expansion as values obtained from different crystalline axes would be expected to exhibit considerable variation. There is also quite a spread in the reported values for thermal expansion coefficient of HMX. HMX does not exhibit significant asymmetry in its expansion, so that should not contribute to the variation.

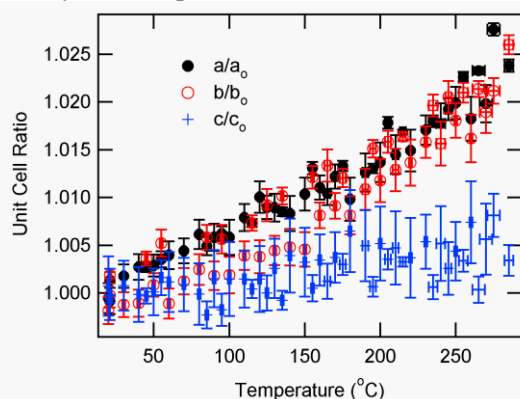


**Figure 5.** Unit cell length ratios as a function of temperature for HNS.

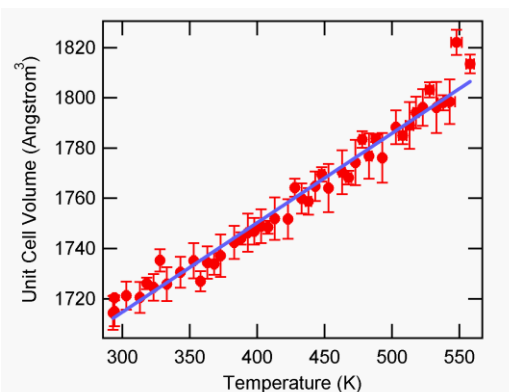


**Figure 6.** Unit cell volume as a function of temperature for HNS. A linear fit to the data is shown as a solid line.

**Table 2.** Comparison of values for volume thermal expansion from this work and other cited works.

	$\alpha$ ( $K^{-1}$ )
HMX	0.00027
HMX (Herman <sup>16</sup> )	0.00013
HMX (Saw <sup>17</sup> )	0.0002
HNS	0.00021
LLM-105	0.000209
TATB	0.00019
TATB (Saw, single crystal <sup>18</sup> )	0.000101
$\epsilon$ CL-20	0.000104

### 3.4 Correlation to explosive sensitivity

Figure 7 shows views of the lattice stacking for the three materials [19,20,21] which exhibited asymmetric compression and expansion in this work. All three exhibit a layered nature to their

stacking. This layering occurs along specific axes, which correspond to the axes exhibiting the extremes in compression and expansion.

Table 3 lists values for impact and friction sensitivity for energetic ingredients in this study taken from the Naval Surface Warfare Center IHEODTD sensitivity database. Impact testing uses a ball dropped from various heights to illicit a response from the sample. Friction testing typically drags a wheel or peg across the sample to generate a response. Sensitivity database values are dependent on equipment and operator differences as the criteria for a sample “response” can vary. Therefore, comparison of absolute values from one database to another is not appropriate, but the general sensitivity trends between materials should remain consistent. There are a range of values listed for each material in table 3 because samples were tested at multiple times and from multiple sources. HNS in a pure powder form was not listed in the database, so its sensitivity is listed relative to other materials on the table from comparison with other databases. The values for impact and friction sensitivity show that sensitivity is lower for the three energetic ingredients that exhibit layered nature to their lattice stacking (TATB, HNS, and LLM-105). It does not appear that an extension of this correlation can be made to any trends in the values for bulk moduli or volume thermal expansion coefficients, but it does appear to be associated with the asymmetric compression and expansion of the unit cell axes. Therefore, it could be possible to correlate data from unit cell axis compression to anticipated trends in impact and friction sensitivity.

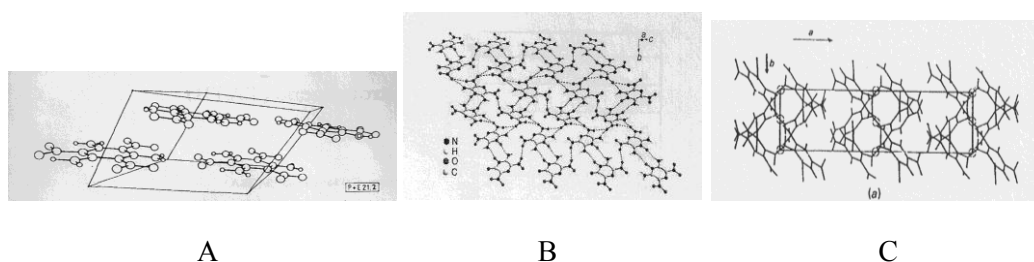


**Figure 7.** Lattice planes for A) TATB<sup>19</sup>, B) LLM-105<sup>20</sup>, and C) HNS<sup>21</sup>, emphasizing the layered nature of the stacking in these materials.

**Table 3.** Values for impact and friction sensitivity tests for various energetic materials.

	ERL Impact (cm)	ABL Friction 8 ft/s, psig
HMX	13-35	<30-135
$\epsilon$ CL-20	9-12	<30-50
LLM-105	89->320	>980
TATB	>320	160 (BAM)
HNS	Between HMX and TATB	

#### 4. Conclusions

Angle dispersive x-ray diffraction experiments were conducted on HMX, CL-20, LLM-105, TATB, and HNS at high pressures and temperatures using diamond anvil cells. Phase changes were observed in the pressure and temperature range investigated for HMX and CL-20. HMX exhibited a change from the beta phase to the delta phase upon decompression at 140 °C under non-hydrostatic conditions. The epsilon phase of CL-20 exhibited changes to both the gamma and zeta phases; however, the zeta phase was not recoverable to ambient conditions. Data from x-ray diffraction experiments were analyzed and fit to obtain bulk modulus, its first pressure derivative, and volume thermal expansion coefficient values. Asymmetry in the compression and expansion of the unit cell axes was observed for LLM-105, HNS, and TATB. This asymmetric expansion and compression results from the layered nature of the lattice plane stacking and can be correlated to impact and friction sensitivity data for these materials.

### Acknowledgements

X-ray diffraction data were collected at the Cornell High Energy Synchrotron Source (CHESS). CHESS is supported by the National Science Foundation and the National Institutes of Health/National Institute of General Medical Sciences under award DMR-0225180.

This work represents an effort spanning approximately ten years. Many colleagues assisted in the collection and analysis of the data reported. The author would like to thank Suhithi Peiris, Chad Stoltz, Brian Mason, Chak Wong, Benjamin Freedman, Jason Ball, and Emily Heim for much assistance and support.

### References

- [1] Gump J C and Peiris S M 2005 *J. Appl. Phys.* **97** 053513
- [2] Gump J C and Peiris S M 2008 *J. Appl. Phys.* **104** 083509
- [3] Gump J C et al. 2011 *J. Appl. Phys.* **110** 073523
- [4] Gump J C et al. 2010 *Proc. 14<sup>th</sup> Int. Det. Symp.* 871-877
- [5] Gump J C, Stoltz C A, Mason B P and Heim E 2012 *AIP Conf. Proc.* **1426** 575-8
- [6] Peimarini G J, private communication
- [7] Bassett W A, Shen A H, Bucknum M and Chou I M 1993 *Rev. Sci. Instrum.* **64** 2340-5
- [8] Chijioke A D, Nellis W J, Soldatov A and Silvera I F 2005 *J. Appl. Phys.* **98** 114905
- [9] Largarec K and Desgreniers S 1994-97 Simplified Image Plate Software
- [10] Cooper P W and Kurowski S R 1996 (Wiley-VCH; New York, NY)
- [11] Russell T P, Miller P J, Piermarini G J and Block S 1992 *J. Phys. Chem.-US* **96** 5509-12
- [12] Russell T P, Miller P J, Piermarini G J and Block S 1993 *J. Phys. Chem.-US* **97** 1993-7
- [13] Cohen R E, Gulseren O and Hemley R J 2000 *Am. Mineral.* **85** 338-344
- [14] Yoo C S and Cynn H 1999 *J. Chem. Phys.* **111** 10229-10235
- [15] Stevens L, Velisavljevic N, Hooks D and Dattelbaum D 2008 *Propell. Explos. Pyrot.* **33** 286-95
- [16] Hermann M, Engel W and Eisenreich N 1992 *Propell. Explos. Pyrot.* **17** 190-195
- [17] Saw C 2002 *Proc. 12<sup>th</sup> Int. Det. Symp.* 70-78
- [18] Saw C K, Zaug J M, Farber D L, Weeks B L and Aracne C M 2002 *AIP Conf. Proc.* **620** 856-9
- [19] Kolb J and Rizzo H 1979 *Propell. Explos. Pyrot.* **4** 10-16
- [20] Ma H, Song J, Zhao F, Gao H and Hu R 2008 *Chinese J. Chem.* **26** 1997-2002
- [21] Gerard P F and Hardy A 1988 TNT *Acta Crystallogr. C* **44** 1283-7